In vitro localisation of intracranial haematoma using electrical impedance tomography semi-array

S. Bentolhoda Ayati, Kaddour Bouazza-Marouf, David Kerr

Wolfson School of Mechanical and Manufacturing Engineering, Loughborough University, Loughborough, LE11 3TU, United Kingdom

Abstract

Electrical Impedance Tomography is a non-invasive and portable method that has good potential as an alternative to the conventional modalities for early detection of intracranial haematomas in high risk patients. Early diagnosis can reduce treatment delays and most significantly can impact patient outcomes. Two eight-electrode layouts, a standard ring full array (FA) and a semi-array (SA), were investigated for their ability to detect, localise and quantify simulated intracranial haematomas *in vitro* on ovine models for the purpose of early diagnosis. SA layout speeds up electrode application and avoids the need to move and lift the patient's head. Haematomas were simulated using gel samples with the same conductivity as blood. Both layouts, FA and SA, could detect the presence of haematomas at any location within the skull. The mean of the relative radial position error with respect to the brain radius was 7% for FA and 6% for SA, for haematomas close to the electrodes, and 11% for SA for haematomas far from the electrodes at the back of the head. Size estimation was not as good; the worst size estimation error for FA being around 30% while the best for SA was 50% for simulated haematomas close to the electrodes.

Keywords

Electrical impedance tomography, intracranial haematoma, localisation, size estimation

1. Introduction

Head injury is the main cause of death among young adults and children and may become the third greatest global death cause by 2020, due to the substantial number of associated deaths and cases of disability [1]. The UK National Confidential Enquiry into Patient, Outcome and Death (NCEPOD) reported that more than half of patients that required neurosurgical advice were taken to hospitals with no on-site neurosurgical provision and only 14% of patients requiring secondary transfer to a neurosurgical centre had access to neurosurgical treatment within four hours [2]. Patients treated in a non-neurosurgical centre had a 26% increase in mortality and a 2.15 fold increase in the risk of death compared to patients treated at a neurosurgical centre [3]. First responders need more information on the neurological condition of their patient. In particular, they require information on potentially evolving haematomas which may need prompt and rapid action. This information is vital for proper triage, and to ensure the best possible decisions are made for the patient's welfare.

Haematomas expand and increase the intracranial pressure on the brain. A growing haematoma will cause severe and even permanent damage to the delicate tissue of the brain, morbidity, and eventual death of the patient [4]. Haematomas are classified based on their location. Epidural Haematomas form between the skull and the dura-mater. They occur because of trauma and a tear in an artery, often to the temple, where the middle meningeal artery is located. Subdural haematomas occur because of trauma and a tear in veins beneath the dura-mater in the brain. A subdural haematoma is very close to the brain and may cause a serious problem. Intracerebral Haematomas, occur within the brain parenchyma itself due to bleeding from trauma or uncontrolled high blood pressure. The development of the haematoma from benign to symptomatic can be sudden, and a patient can change from lucid to a state of rapid neurological deterioration over a very short-period of time [5]. It is well

47 known that the time from injury-to-diagnosis-to-treatment is a key factor in patient outcome,

48 and must be minimised for a patient to make a full recovery.

49 Electrical Impedance Tomography (EIT) reconstructs cross-sectional images of the

50 conductivity distribution of the internal components of the brain, based on non-invasive

51 voltage measurements through an array of electrodes on its boundary. Blood has a high

52 electrical conductivity contrast relative to other cranial tissues and thus its appearance can be

53 detected and monitored using EIT [6].

54 Head injuries and haematoma are often accompanied by other traumatic injuries that can be

55 aggravated by unnecessary movement, including the placing of electrodes around the head.

56 Therefore, it is desirable to develop methods that do not involve applying electrodes at the

57 back of the head. Placement of the electrodes on the anterior of the head avoids exacerbating

58 existing injuries and removes the need to lift the patient. However, good localization of a

59 haematoma is hampered by eliminating the electrodes at the back of the head. To conquer the

60 quality reduction of the images and to minimize these errors, several reconstruction strategies

61 have been proposed previously [7]. The purpose of this study is to evaluate the performance

62 of EIT, using optimised eight-electrode configurations. This includes an investigation of the

63 different configurations to evaluate their ability to detect and localise anomalies similar to

64 haematoma in the human head, for the purpose of early diagnosis. Using the minimum

65 number of electrodes is always desirable in clinical applications since it may also speed up

66 the electrode setup process in emergency cases. The proposed electrode configurations are

67 evaluated for the detection and localisation of simulated haematomas *in vitro* using an ovine

68 model. Intracerebral haematoma detection has been considered in previous studies using EIT

69 [8]. Epidural and subdural haematomas are considered in this study since their location can

70 represent the worst case with respect to the SA configuration.

2. Methods

In EIT, the process is divided into a forward problem and an inverse problem. To reconstruct the conductivity distribution images through the EIT inverse problem the forward problem on a prototype model has to be solved. For general cases, a numerical method such as finite element analysis is required to implement the model and solve the forward problem. Initially, a simple forward model based on a circular shape with a homogenous conductivity distribution may be used to calculate the sensitivity matrices [9]. Better results are obtained if the forward model exactly matches the object in terms of internal conductivity distribution and external geometry. In principle, an incorrect estimate of boundary shape will introduce artefacts and reduce the quality of the reconstructed images. However, more realistic models need to be used carefully since inaccurate prior information may yield images worse than those reconstructed with a simple forward model [10]. In practice, it is difficult to specify an accurate model for an individual head because head geometry varies from patient to patient.

2.1. Full and semi-array electrode layouts

In this study, two eight-electrode layout strategies were investigated *in vitro* and compared in terms of their ability to detect and localise intracranial haematomas. The first one was a standard ring layout or full-array (Figure 1a), where the eight electrodes were placed equally spaced around the head. The second layout was a novel electrode configuration applied to the front of the head. This so-called semi-array (SA) configuration consisted of a set of eight electrodes separated by angle of $36°$ in a semi-circular profile (Figure 1b). This layout simplifies the application of the electrodes and avoids the need to move and lift the patient's head. An adjacent current pattern was applied to both layouts, wherein current was applied in turn to pairs of adjacent electrodes, and voltages were measured across other pairs of adjacent electrodes. In the SA, use of this scheme included measurements and current applications

95 between the last-numbered and first electrodes positioned at the end of the array and

96 approximately 108° apart. Both layouts involved 8 current positions and a total of 40 voltage

97 measurements. Experiments were performed on an ovine model using both layouts and the

98 results obtained from the SA layout were compared with data from the standard eight-

99 electrode full-array (FA) layout to determine the ability of the SA to detect and localise

100 intracranial haematomas. Restricting electrodes at the back of the head limits the resolution

101 and thus inferior localisation of the anomaly can be expected, compared to that of the FA

102 layout.

103   2.2.Data generation

104 *In vitro* ovine experiments were performed in conjunction with an eight-electrode EIT system

105 to determine the potential of this configuration to provide good results *in vivo*. To obtain the

106 experimental measurements, a prototype 16-electrode EIT system known as the "EITLboro"

107 rig was used. The structure of this device is presented in Figure 2. The system is controlled

108 by a microcontroller connected to a PC through a serial port. A graphical user interface was

109 developed using Visual Basic (VB). A sinusoidal current generated by a constant current

110 source was injected through one pair of adjacent electrodes and the corresponding boundary

111 potentials were measured over pairs of the remainder of the neighbouring electrodes using a

112 multiplexer. The input pair of electrodes was switched over all adjacent electrodes pairs and

113 the measurement procedure was repeated for all possible adjacent pairs. The performance of

114 this system was previously evaluated using phantom experiments [11]. The results showed a

115 high level of accuracy with an average accuracy of 93.5% for the system. This EIT system

116 has 16 channels and operates with a temporal resolution of 100 frames per second. For this

117 experiment, a constant current of 1mA at a frequency of 50 kHz and 8 electrodes were chosen.

5

2.3.Experimental setup

119 Five freshly skinned sheep heads (labelled as A, B, C, D and E) were obtained from a local

120 butcher. The locations of the 8 electrodes for each layout were marked in different colours on

121 the skull. Equal distance between electrodes has been considered around the head for the FA

122 and in the anterior of the head for the SA according to the perimeter measurement of each

123 head. Eight Ag/AgCl disk electrodes (Unimed Electrode Supplies Ltd) were fastened to the

124 skull using conductive paste (Unimed Electrode Supplies Ltd) for the FA layout (Figure 3a).

125 These electrodes were also soldered to the wires to connect to the skull on the interior of the

126 head using conductive paste for the SA layout (Figure 3b).

127 A saline solution with the same conductivity as blood (0.67 S/m) was made with a

128 concentration of 0.33% [weight/volume] of sodium chloride in water. In order to localise

129 haematoma *in vitro*, the position of the anomaly has to be known with a good estimation. To

130 simulate a more realistic haematoma in an accurate location, the saline solution was

131 transformed to gel. The saline solution was stirred using a magnetic stir bar at a temperature

132 of 70°C while agar powder was added to achieve the desired gel concentration (1.9% by

133 weight). Then the solution was poured into a 1 cm diameter tube and allowed to cool at room

134 temperature. The gel sample was removed from the tube and cut into one tenth of the

135 diameter of each brain to simulate pockets of blood. The conductivity of the gel sample was

136 measured and found to be the same as the conductivity of the saline solution. A 2-terminal

137 measurement was performed to measure the gel conductivity and the same gel samples were

138 used on each subject. An AC voltage was applied across the gel at a frequency of 50 kHz at

139 room temperature using a waveform function generator connected in series with a digital

140 multimeter to measure the AC current and voltage across the gel. The circuit was calibrated

141 with multiple known resistances, and the conductivity measurements were compared to

142 published data [12].

143 All the skulls were cut in approximately half using a bone saw. The top half of the skull was

144 carefully removed and the brain was exposed in order to position the anomalies (Figure 4).

145 Gel samples were placed superficially on top of the brain lobe and the top half of the skull

146 was replaced. The anomaly was located in different positions along the α, αβ, β, βγ and γ axes

147 (at θ = 0°, 45°, 90°, 135° and 180°), with the anomaly centre placed successively at a relative

148 radial displacement of 0.8 from the brain centre. Five locations were considered in total as

149 shown in Figure 1 and the measurements performed using both layouts for each anomaly to

150 study reconstruction, detection and localisation characteristics. The aim was to study and

151 compare the ability of the SA and FA layouts to detect and localise these anomalies,

152 especially for the SA, and to evaluate the dependency of the results on the distance of the

153 anomaly from the electrodes.

154   2.4.Reconstruction

155 In this study, EIT difference images were reconstructed based on the assumption that the

156 conductivity changes are small enough. The relationship between the boundary voltage

157 measurement changes and internal conductivity changes can be expressed with a sensitivity

158 matrix (S) as in Eq. (1). S was calculated from forward solutions of a two-dimensional disk

159 finite element model with a homogenous conductivity distribution [9].

160 $\Delta V = S \ \Delta \sigma$ (1)

161 Conductivity changes ($\Delta\sigma$) can be determined by inverting the sensitivity matrix; however, S

162 is ill-conditioned and not square. Since the EIT inverse problem is severely ill-posed and a

163 small amount of noise on boundary measurements, ΔV, can cause a large oscillation for the

164 solution, a regularization technique was used to reduce this effect by improving the condition

165 of S [6].The Truncated Singular Value Decomposition (TSVD) method which has previously

166 been identified as a suitable regularization method [13] was used to regularize the inversion

167 of the sensitivity matrix. The truncation point k needs to be chosen carefully, less than or

168 equal to the rank of the matrix, as it would otherwise produce inaccurate images. The

169 truncation point was chosen depending on the noise level in the voltage measurements and

170 the rank of the sensitivity matrix on inspection of the L-curve of experimental data [14]. The

171 truncation numbers were almost the same for all the datasets. The pseudo-inversion ($S^{\dagger}$) was

172 achieved using TSVD and images were obtained using Eq. (2).

173 $\Delta\sigma = S^{\dagger}\Delta V$ (2)

174 In the SA, measurement sensitivity depends strongly on the anomaly location since the

175 electrodes are not placed all over the head. Some reconstructed anomalies located far from

176 the electrodes in the posterior region were almost invisible or erroneous when TSVD

177 reconstruction was used. Therefore, in order to enhance image reconstruction quality and

178 improve anomaly localisation, the sensitivity matrix was weighted with a diagonal matrix

179 composed of a system blurring property, which was directly calculated from the sensitivity

180 matrix [7]. In the Weighted Pseudo-Inverse (WPI) method, reconstruction was weighted with

181 P prior to pseudo-inversion. The entries of a diagonal weighting matrix (P) were calculated

182 using Eq. (3) where ne is the total number of elements. The blur matrix (B) is dimensionless

183 and can be pre-calculated from the sensitivity matrix S via Eq. (4). Then the reconstruction

184 was modified to obtain images using Eq. (5).

$$p_j = \left(\sum_{i=1}^{ne} B_{ij}^2 \right)^{-1}$$ (3)

185

$$B = S^{\dagger}S$$ (4)

186

187 $\Delta\sigma = (SP)^{\dagger}\Delta V$ (5)

188   2.5.Localisation

189   The position of the anomaly (x,y) can be estimated from the reconstructed images by

190   averaging the positions of all elements, weighted by their conductivity changes [8] via Eqs. (6)

191   and (7):

$$x = \frac{\sum_{i=1}^{ne} \Delta\sigma_i a_i x_i}{\sum_{i=1}^{ne} \Delta\sigma_i a_i} \tag{6}$$

$$y = \frac{\sum_{i=1}^{ne} \Delta\sigma_i a_i y_i}{\sum_{i=1}^{ne} \Delta\sigma_i a_i} \tag{7}$$

192   The anomaly location (x, y) is effectively the centre of the reconstructed anomaly. The values

193   x_i and y_i are the coordinates of the centre and a_i is the area of each element. The difference

194   between the actual position of the anomaly and its reconstructed location within the xy plane

195   can be calculated as the absolute location errors (relative radial error, D_{xy}) quoted as a

196   fraction of the brain radius, R, [8] via Eq. (8):

$$D_{xy} = \frac{\sqrt{(\Delta x)^2 + (\Delta y)^2}}{R} \tag{8}$$

197   2.6.Quantification

198   The anomaly size was assessed with a characteristic parameter, the quantity index (QI),

199   defined in Eq. 9 as an EIT image parameter that correlates with the anomaly size [15]. The

200   quantity index is the sum of conductivity change multiplied by the area of the element over

201   the image area:

$$QI = \sum_{i=1}^{ne} \Delta\sigma_i a_i \tag{9}$$

202   where, for an element (or pixel) i, $\Delta\sigma_i$ is the conductivity change reconstructed in the *i-th*

203   element. QI values should be constant since the anomaly sizes are the same during the

204   experiment over all the positions.

3. Results

The data for intracranial haematomas in five ovine models were successfully collected with the EITLboro rig and used to reconstruct the images. To improve the SNR of EIT, a sequence of at least 100 frames of data was collected before the anomalies were introduced. These were averaged and used as the reference data set. For each anomaly position, 100 frames of data were collected and averaged as the perturbation data for that anomaly position.

3.1. Comparing FA and SA localisation

The simulated haematomas were localised using the reconstructed images. The results of the anomaly localisation in the five ovine models using both FA and SA layouts are presented in Figures 5 and 6 respectively. The position of the simulated haematomas varied as a function of angle from 0° to 180° with 45° increments at relative radial displacement of 0.8 from the brain centre. Locations were normalized to a circular shape with unit diameter. The discrepancy between the actual and reconstructed locations is illustrated by arrows. For illustration, reconstructed images of the anomalies in subject E using FA configuration are shown in Figure 5 and reconstructed images of the anomalies in subject C using SA configuration are shown in Figure 6. The simulated anomalies were detected for all the positions using both layouts; however FA results were in general superior to the SA results. Relative radial localisation errors for five ovine models using FA and SA are shown in Figures 7 and 8 respectively. As expected, the SA layout localised simulated anomalies as well as the FA layout apart from the anomalies placed far away from the electrodes. Localisation errors were larger for reconstructions of the anomalies at 135° with the worst value of D_{xy} being 0.3265 using the SA layout, and 0.0828 using the FA layout, both values being with respect to unit radius. The mean and variance of the relative radial errors are presented in table 1. Both the FA and SA electrode layouts could localise simulated

229 haematomas well, producing a maximum mean relative radial error of 0.0714 and 0.2364

230 respectively at 135° with respect to the unit radius.

3.2. Comparing FA and SA size estimation

232 The reconstructed images of the simulated haematomas were gathered and post-processed to

233 determine QI values. The ability of the FA and SA layouts to quantify these anomaly sizes

234 was compared to the actual QI. The normalized QI values for five ovine models using the FA

235 electrode layout over the image plane against anomaly position for five angles are shown in

236 Figure 9. For the SA layout, the same positions of anomalies in directions of α, αβ, β, βγ and

237 γ were used. Normalized QI values from the SA reconstructions of simulated anomalies are

238 shown in Figure 10. Size estimation results for the FA layout are superior to those for the SA

239 layout. The worst QI error in reconstructions using the FA layout was around 30%.

240 According to the reconstructed images, the size of the simulated anomalies at 0° and 45° (α

241 and αβ) are measured by maximum error of approximately 55% and 50% respectively in the

242 case of the SA electrode layout. For simulated anomalies placed at 90° (β) using the SA

243 layout, although in one case the QI value is large, the worst QI error in the others is about

244 55%. The SA layout performance to quantify the simulated anomalies at 135° and 180° (βγ

245 and γ) is very poor as in the worst case the anomaly sizes were measured almost three times

246 bigger than their actual size.

4. Discussion

4.1. Comparison between full array and semi-array layouts

249 For the first time, animal studies were performed using EIT to detect and localize

250 haematomas within the skull in an ovine model. In five sheep heads, haematomas were

251 simulated by placing gel samples with the same conductivity as blood at different positions.

252 Two eight-electrode layouts were applied to compare their ability to localise and quantify the

11

253   simulated haematomas. An optimised, novel electrode layout named semi-array (SA) was

254   introduced and its performance was evaluated and compared *in vitro* with a conventional full

255   array electrode layout. The FA layout performed well in both localisation and size estimation

256   of the anomalies. We believe that the errors in the FA experiments are due to the presence of

257   random and systematic experimental noise. As expected, the SA layout performed well in

258   detecting and localising anomalies close to the electrodes, but slightly worse for anomalies

259   far away from the electrodes. Reduction of the electrodes at the posterior of the head reduced

260   overall image quality and increased uncertainty in estimations of location and size of the

261   anomalies. Large spatial variance and therefore the variability in size estimates of an anomaly

262   because of the restricted number of electrodes at the posterior of the head are inevitable. We

263   believe that the large size estimation errors may have been caused by the noise-generated

264   artefacts in reconstructions and the electrode positions.

265   4.2.Anomaly size estimation

266   Although QI values depend on the size of the anomaly, the regularisation method and the

267   sensitivity matrix calculation also affect the size estimation. The FA and SA electrode layouts

268   produce different sensitivities in the region at the back of the head and therefore have

269   different QI accuracy. Large size errors in SA may have been related to the smaller sensitivity

270   at the posterior region of the head, far from the electrodes, combined with measurement noise.

271   However, spatial variation of QI was improved by using blurring properties calculated

272   directly from the sensitivity matrix. The truncation number for each case was chosen based

273   on the noise level in the voltage measurements and the rank of the sensitivity matrix on

274   inspection of the L-curve of experimental data.

275   4.3.Comparing results with earlier studies

276   Using EIT for clinical applications to detect and image bleeding in an animal model has been

277   proven in previous studies [16, 17]. A group based at the University of Florida has applied

278 EIT to detect intra-ventricular haemorrhage (IVH) for neonate applications [8]. In their

279 phantom experimental studies, data were collected by a FA layout with 16 electrodes equally

280 spaced around the head, using adjacent current patterns. Their results showed a maximum

281 radial error of 0.1 and QI error of 30% which is better than our size estimation accuracy.

282 Sadleir *et al.* [6] introduced a hemi-array electrode layout for the application of abdominal

283 trauma. QI values of their phantom experimental studies showed a variation of around a

284 factor of 4, the maximum being 220%. Hemi-arrays have been used in vivo to quantify

285 accumulating abdominal fluid [18] and to monitor lung resistivity by *Zlochiver et al* [19].

286 However, the hemi-array electrode layout failed in our application to detect simulated

287 haematomas using ovine models. We believe that the presence of the skull and the geometry

288 structure of the head may restrict the use of the hemi-array in this application. However, our

289 optimised SA electrode layout has shown its reliability to detect, localise and quantify the

290 simulated haematomas in this application. According to earlier studies [20, 21], the quality

291 of the images and consequently the localisation and size errors may be improved by

292 increasing the number of electrodes. However, the objective of this concept is to optimize the

293 number and position of the electrodes in order to speed up the electrode setup process and

294 avoid the need to move and lift the patient's head in emergency cases. We believe that using

295 an eight-electrode configuration is more preferable than using 16 or 32 and that the ensuing

296 results are quite acceptable. Although the use of 2D imaging restricts the z direction

297 localisation, the overall process is faster and the results are reliable enough for a useful

298 application to emergency cases.

299   4.4.Comparing EIT with current modalities

300 Haematomas are typically diagnosed by neurological assessment in the emergency room

301 followed by a Computed Tomography (CT) scan. CT scanners are not portable and thus

302 diagnosis cannot be made until the patient is delivered to the hospital. Moreover, CT

303 scanning is not always available for 24 hours a day, and in cases of multiple traumas, it may

304 not be possible to scan the patient until they have been adequately stabilised [22]. Although

305 the sensitivity and resolution of Magnetic Resonance Imaging (MRI) is higher than CT, the

306 transporting requirement of ill patients and equipment compatibility restrict use of this

307 method. EIT is a non-invasive, portable, low-cost, operator independent method that has the

308 potential to monitor and measure the progress of internal bleeding. EIT offers a good

309 alternative to the conventional modalities for early detection, localisation and size estimation

310 of haematomas in high risk patients. Early diagnosis can reduce treatment delays, save on

311 costs and waste, and most significantly, positively impact patient outcomes. Treatment delays

312 can thus be mitigated by giving better and earlier information on haematomas at the triage

313 stage.

314 **5. Conclusion**

315 This study indicates the feasibility of detection, localisation and size estimation of

316 haematomas *in vitro* with preliminary EIT imaging on ovine models for the purpose of early

317 diagnosis. Two eight-electrode layouts were compared *in vitro* on their ability to detect,

318 localise and quantify simulated haematomas. As expected, the FA layout was found to be

319 more robust than the SA layout, having an overall better quality on localisation and size

320 estimation of the simulated haematomas. Although using the SA configuration reduces the

321 sensitivity and accuracy of quantity estimations, an optimized electrode layout that does not

322 require the patient to be lifted for its application would be very convenient for emergency

323 applications where the required accuracy is not critical.

References

[1] Dinsmore J. Traumatic brain injury: an evidence-based review of management. Continuing Education in Anaesthesia, Critical Care & Pain Advance Access 2013.

[2] Treasure T. Trauma: Who cares? A report of the National Confidential Enquiry into Patient Outcome and Death (NCEPOD) 2007:19.

[3] Patel H, Bouamra O, Woodford M, King A, Yates D, Lecky F, On behalf of the Trauma Audit and Research Network. Trends in head injury outcome from 1989 to 2003 and the effect of neurosurgical care: an observational study. The Lancet 2005;366(9496):1538-44.

[4] Voss M, Knottenbelt J, Peden M. Patients who reattend after head injury: a high risk group. BMJ 1995;311(7017):1395-98.

[5] Moore K, Dalley A, Agur A. Clinically Oriented Anatomy. Wolters Kluwer Health/Lippincott Williams & Wilkins 2010:876-77.

[6] Holder D. Electrical impedance tomography methods, history and applications. UK: IOP Publishing 2005.

[7] Sadleir R, Zhang S, Tucker A, Oh S. Imaging and quantification of anomaly volume using an eight-electrode 'hemiarray' EIT reconstruction method. Physiological Measurement 2008;29:913–27.

[8] Tang T, Oh S, Sadlier R. A robust current pattern for the detection of intraventricular hemorrhage in neonates using electrical impedance tomography. Ann Biomed Eng 2010;38(8):2733-47.

[9] Bagshaw A, Liston A, Bayford R, Tizzard A, Gibson A, Tidswell A, Sparkes M, Dehghani H, Binnie C, Holder D. Electrical impedance tomography of human brain function using reconstruction algorithms based on the finite element method. Neuroimage 2003;20(2):752-64.

[10] Liston A, Bayford R, Holder D. The effect of layers in imaging brain function using electrical impedance tomography. Physiological Measurement, 2004;25:143-58.

[11] Ayati S, Bouazza-Marouf K, Kerr D, O'Toole M. Performance evaluation of a digital electrical impedance tomography system. Proceedings of the IASTED international symposia in imaging and signal processing in health care and technology, Baltimore, USA, 2012:101-5.

[12] Kandadai M, Raymond J, Shaw G. Comparison of electrical conductivities of various brain phantom gels: Developing a 'brain gel model'. Materials Science and Engineering C 2012;32:2664-2667.

[13] Oh S, Tang T, Tucker A, Sadleir R. Normalization of a spatially variant image reconstruction problem in electrical impedance tomography using system blurring properties. Physiological Measurement 2009;30(3):275–89.

[14] Hansen P, O'Leary D. The use of the L-curve in the regularization of discrete ill-posed problems. SIAM Journal of Science and Computing 1993;14(6):1487–503.

[15] Sadleir R, Fox R. Quantification of blood volume by electrical impedance tomography using a tissue equivalent phantom. Physiological Measurement 1998;19:501–16.

[16] Xu Canhua, Dai Meng *et al.* An optimized strategy for real-time haemorrhage monitoring with electrical impedance tomography. Physiological Measurement 2011; 32(5):585-98.

[17] Xu C-H, Wang L *et al.* Real-time imaging and detection of intracranial haemorrhage by electrical impedance tomography in a piglet model. The Journal of international medical research 2010; 38(5):1596-604.

[18] Tucker A, Ross E, Paugh-Miller J, Sadlier R. In vivo quantification of accumulating abdominal fluid using an electrical impedance tomography hemiarray. Physiological Measurement 2011;32(2):151-65.

[19] Zlochiver S, Arad M, Radai M, Barak-Shinar D, Krief H, Engelman T, Ben-Yehuda R, Adunsky A, Abboud S. A portable bio-impedance system for monitoring lung resistivity. Med Eng Phys 2007;29(1):93-100.

[20] Yvert B, Bertrand O, Thvenet M, Echallier J, Pernier J. A systematic evaluation of the spherical model accuracy in EEG dipole localization. Electroencephalogr Clin Neurophysiol 1997;102:452–59.

[21] Taktak A, Record P, Gadd R, Rolfe P. Data recovery from reduced electrode connection in electrical impedance tomography. Med Eng Phys 1996;18(6):519-522.

[22] Wardlaw J, Lewis S, Sandercock P, Ricci S, Spizzichino L, the I. Why do Italian stroke patients receive CT scans earlier than UK patients? Postgrad Med J. 1999;75(879):18–21.

1 Captions
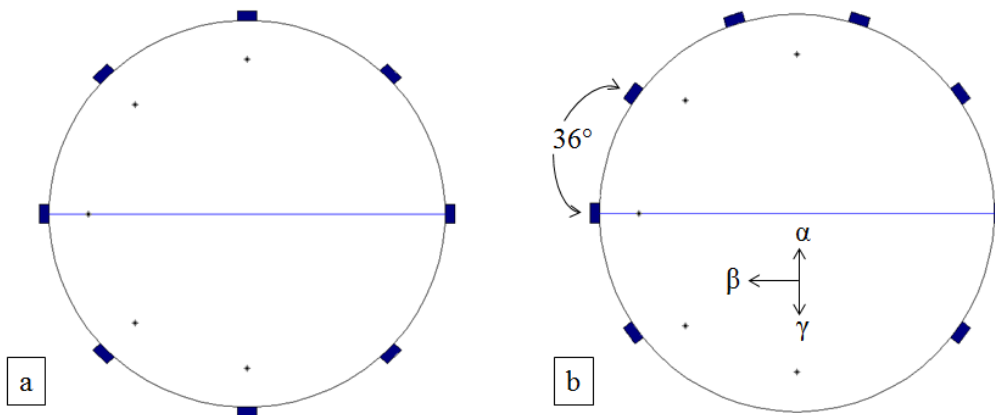
Figure 1: Electrode positions showing (a) the standard ring layout where the eight electrodes were placed equally spaced around the head, and (b) a novel electrode configuration applied to the front of the head separated by angle of 36° in a semi-circular profile. Stars show the ideal positions of centre of simulated anomalies on sheep's head at relative radius of 0.8 in α, αβ, β, βγ and γ axes directions.

8
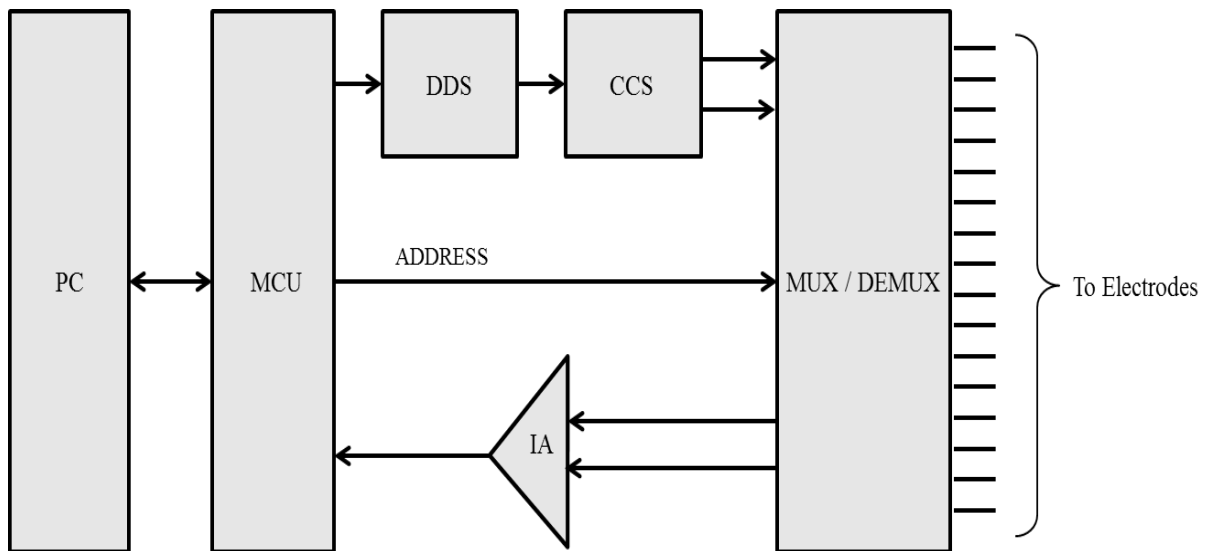
Figure 2: EITLboro architectural overview. This system is based on a microcontroller connected

to a PC through a serial port. A graphical user interface was developed using Visual Basic (VB).

The Constant Current Source, CCS generates a constant current fed by a signal generated by the

Direct Digital Synthesizer, DDS. The measurements were amplified using an Instrumentation

Amplifier (IA) to produce a complete voltage data set.
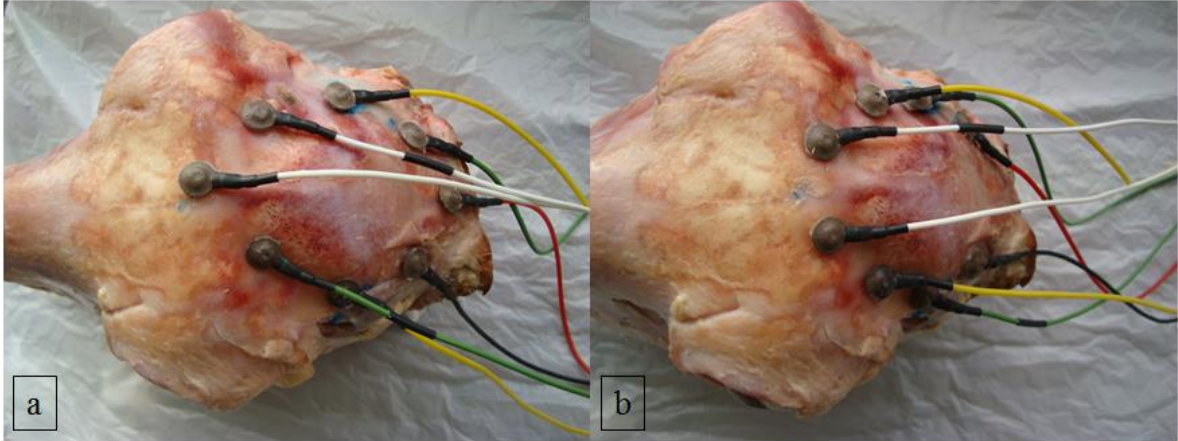
Figure 3: Electrode positions showing (a) eight Ag/AgCl disk electrodes fastened to the skull using conductive paste for full array layout and (b) electrodes connected to the skull on the interior of the head using conductive paste for semi-array layout.
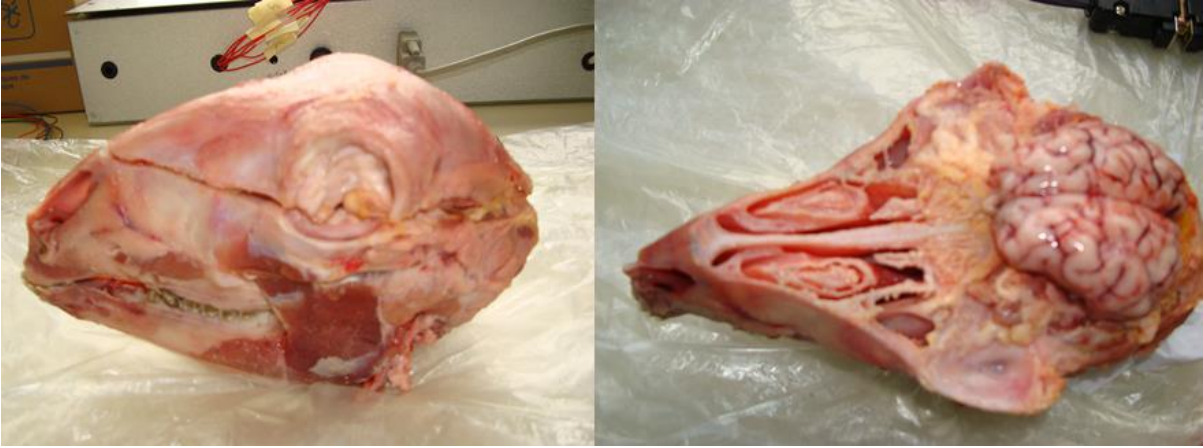
Figure 4: Skulls were cut in approximately half using a bone saw (left). The top half of the skull was carefully removed and the brain was exposed to place the anomalies (right).
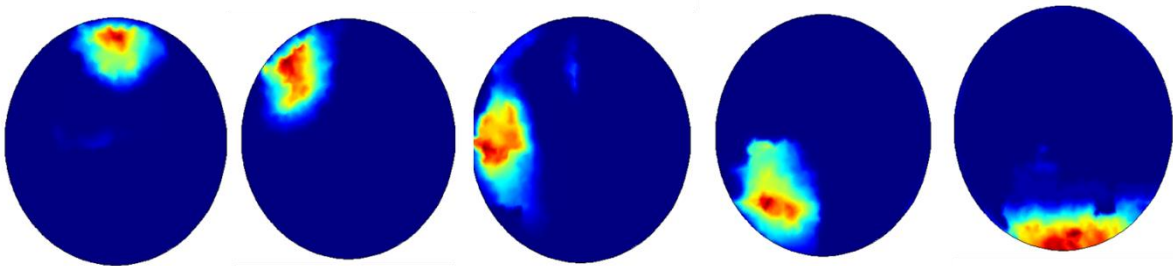
21   (a)

22
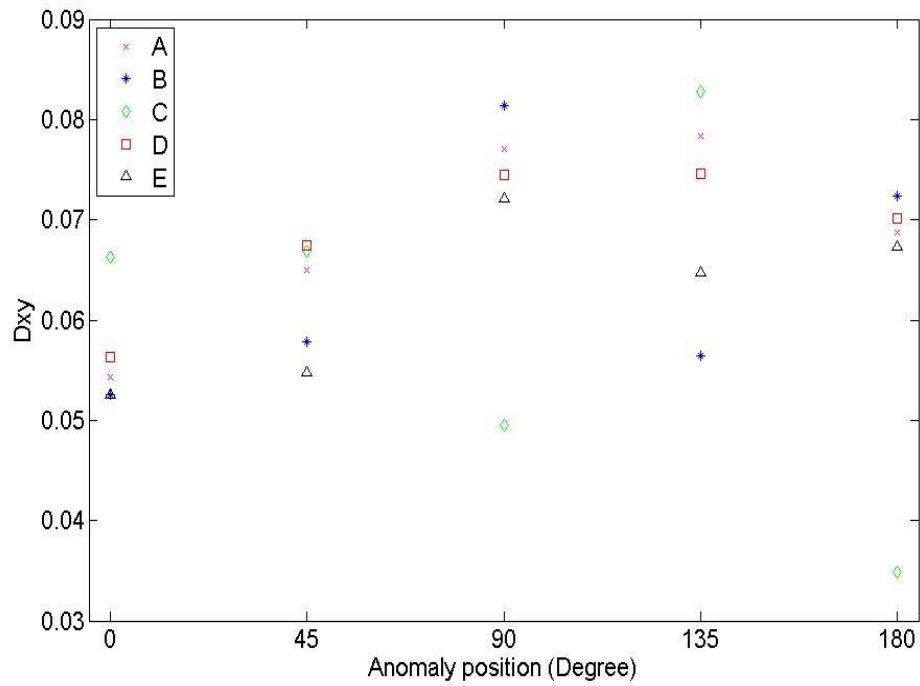
23   (b)
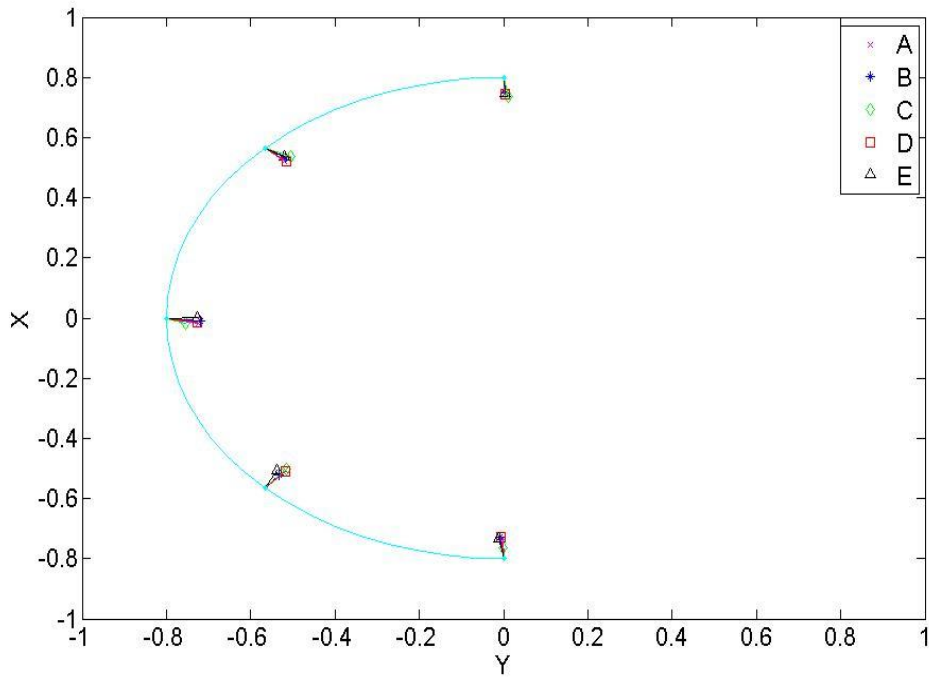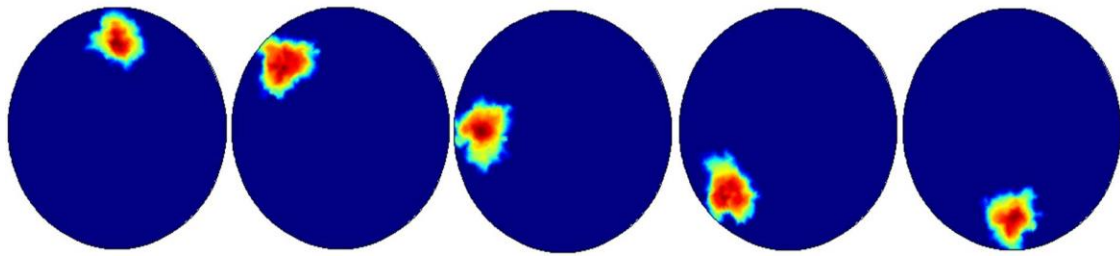
Figure 5: (a) Localization of the simulated anomalies on five sheep's head (A, B, C, D and E) at various positions using full array (FA) electrode layout. Anomaly positions varied as a function of angle (0°, 45°, 90°, 135° and 180°) at relative radius of 0.8.

(b) Reconstructed images of the anomalies in subject E.
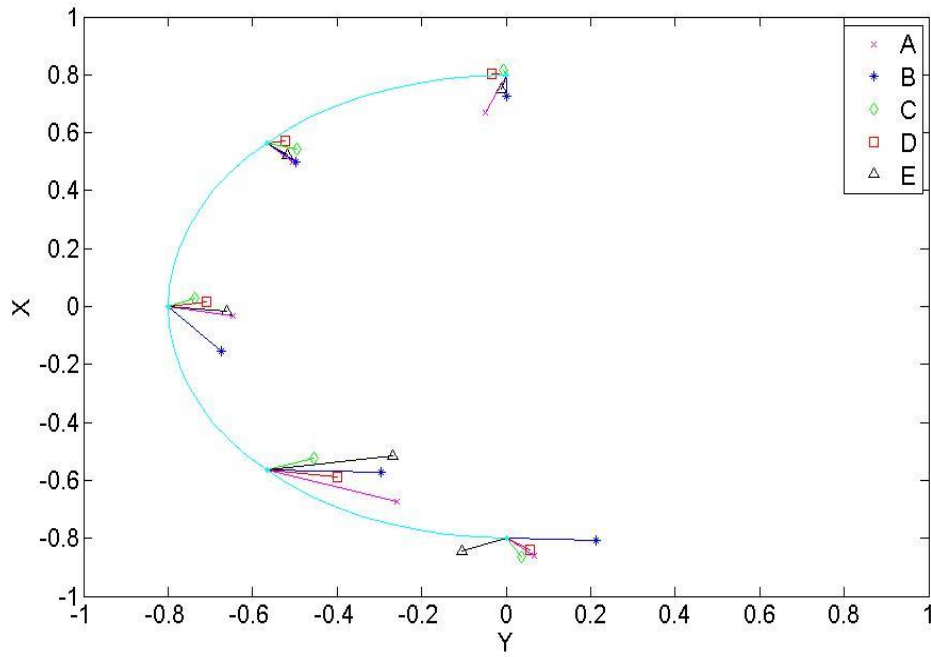
28   (a)

29

30   (b)
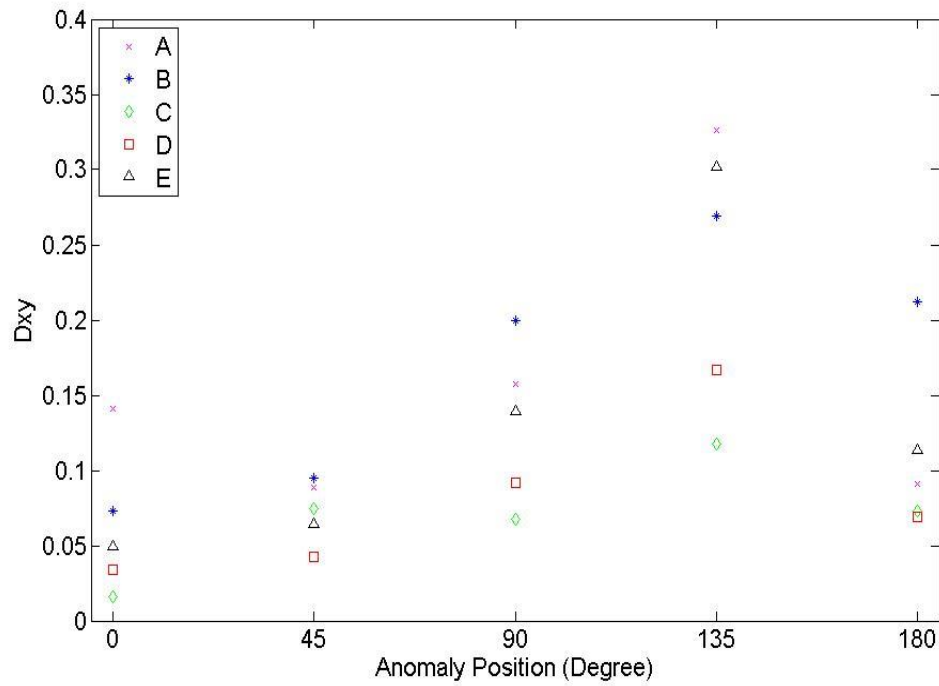
31   **Figure 6:** (a) Localization of the simulated anomalies on five sheep's head (A, B, C, D and E) at

32   various positions using semi-array (SA) electrode layout. Anomaly positions varied as a function

33   of angle (0°, 45°, 90°, 135° and 180°) at relative radius of 0.8.

34   (b) Reconstructed images of the anomalies in subject C.

35

Figure 7: Relative radius localization errors, Dxy, of the simulated anomalies on five sheep's head (A, B, C, D and E) at various positions using full array (FA) electrode layout. Anomaly positions varied as a function of angle (0°, 45°, 90°, 135° and 180°) at relative radius of 0.8.
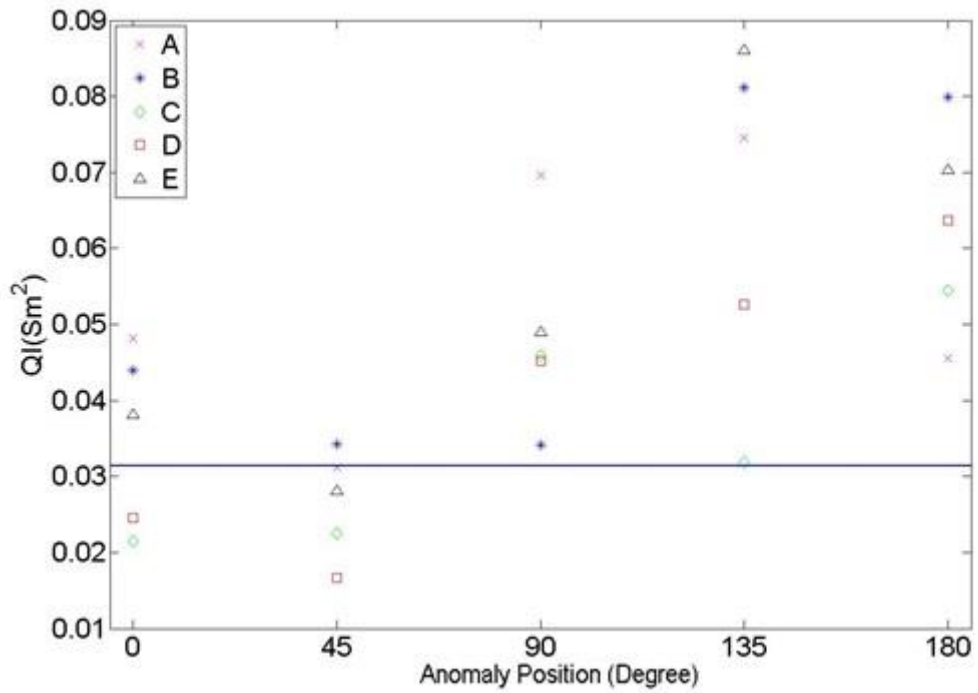
39

Figure 8: Radius relative localization errors, Dxy, of the simulated anomalies on five sheep's head (A, B, C, D and E) at various positions using semi-array (SA) electrode layout. Anomaly positions varied as a function of angle (0°, 45°, 90°, 135° and 180°) at relative radius of 0.8.

43
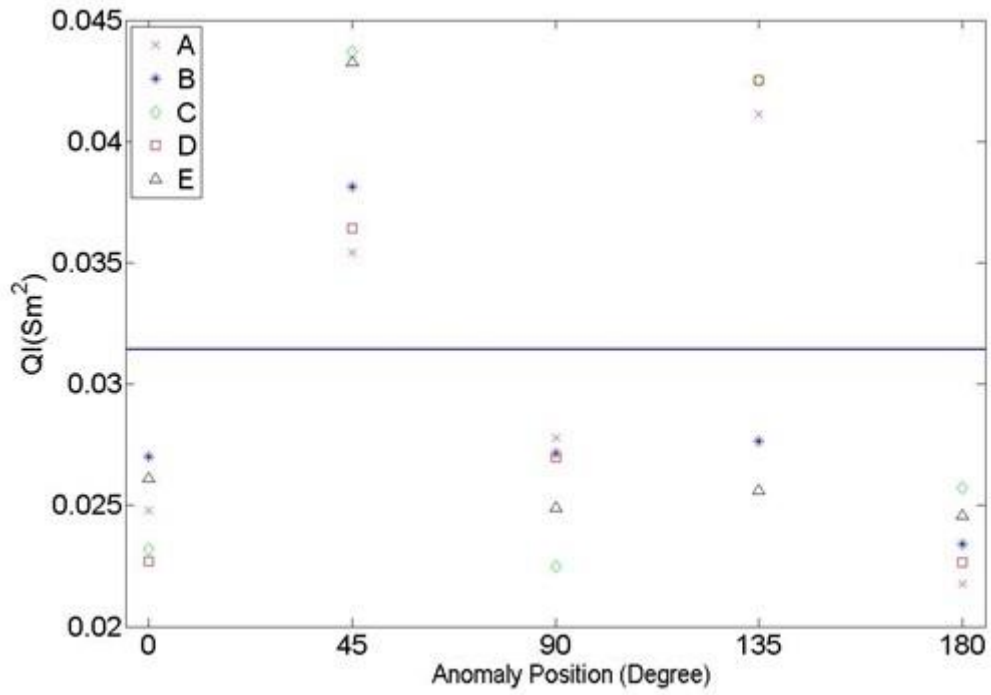
Figure 9: Quantification Indices, QI, of the simulated anomalies on five sheep's head (A, B, C, D and E) at various positions using full array (FA) electrode layout compared with ideal QI. Anomaly positions varied as a function of angle (0°, 45°, 90°, 135° and 180°) at relative radius of 0.8.

48

Figure 10: Quantification Indices, QI, of the simulated anomalies on five sheep's head (A, B, C, D and E) at various positions using semi-array (SA) electrode layout compared with ideal QI. Anomaly positions varied as a function of angle (0°, 45°, 90°, 135° and 180°) at relative radius of 0.8.